

**High-Average-Power Laser Program  
Optics and Chamber Studies:  
Report on Research Performed During FY03**

**M. S. Tillack, F. Najmabadi, A. R. Raffray,  
Z. Dragojlovic, A. C. Gaeris, J. E. Pulsifer, K. Sequoia**

**March 1, 2004**



**Fusion Division  
Center for Energy Research**

University of California, San Diego  
La Jolla, CA 92093-0417

## **ABSTRACT**

This report describes the results of research performed at UC San Diego in support of the High Average Power laser program. Our research focuses on the prediction of chamber and optic responses in inertial fusion energy (IFE) power plants and simulation of those phenomena through modeling and scaled experiments. Progress occurred in three primary topical areas:

(1) Laser-induced damage to grazing-incidence metal mirrors, (2) IFE chamber dynamics and clearing following target explosions, and (3) Chamber wall materials response to pulsed loading by x-rays and high-energy ions.

## **Outline**

1. Task 1: Final Optic Damage Studies
  - 1.1. Statement of purpose
  - 1.2. Background
  - 1.3. Progress in FY03
2. Task 2: Chamber Dynamics & Clearing
  - 2.1. Statement of Purpose
  - 2.2. Background
  - 2.3. Progress in FY03
    - 2.3.1. Simulation Results
    - 2.3.2. SPATRAN upgrades
3. Task 3: Experimental studies of laser-IFE chamber wall
  - 3.1. Statement of Purpose
  - 3.2. Background
  - 3.3. Progress in FY03

# 1. Task 1: Final Optic Damage Studies

## 1.1. Statement of purpose

Our research seeks to develop a better understanding of damage mechanisms and to demonstrate acceptable performance of grazing incidence metal mirrors (GIMM's), with an emphasis on the most critical concerns for laser IFE. Through both experimentation and modeling we will demonstrate the limitations on the operation of reflective optics for IFE chambers under prototypical environmental conditions. In addition, we will work together with other HAPL organizations to develop specific final optic design concepts for a laser-IFE power plant and to field both small and medium scale prototypes for testing. The top level goals for final optics in Phase I are:

1. Meet laser induced damage threshold (LIDT) requirements of more than 5 Joules/cm<sup>2</sup> in large area optics.
2. Develop a credible final optics design that is resistant to degradation from neutrons, x-rays, gamma rays, debris, contamination, and energetic ions.

We are concentrating on grazing incidence aluminum mirrors, as these have shown the most promise for a wider range of wavelengths. Our top level plans include the following three activities:

1. We will quantify the effects of various threats. The full range of damage threats in a laser-IFE power plant includes laser damage, contamination (dust, aerosol and condensate), x-rays, neutrons, and ions. Our work at UC San Diego concentrates on laser-induced damage, including the effects of defects and contaminants on the LIDT. The work includes supporting modeling, with an emphasis on effects of mirror distortion on the wavefront fidelity. We will investigate prototypical designs (*e.g.*, Al-coated SiC) and conditions (*e.g.*, vacuum and non-oxidizing environments), and will investigate the effects of larger area laser spot sizes in collaboration with NRL and LLNL. We plan to complete the threat assessment by the end of FY 2004.
2. We will develop mitigation techniques for those threats that are found to be serious. These techniques include gas puffs, mechanical shutters, and magnetic diversion, depending on the threat. We will initiate these activities in FY 2004, with the needed mitigation schemes identified and evaluated by the end of FY 2005.
3. We will investigate fabrication techniques and integration issues. A reference mirror concept was developed and tested in FY 2003, using pure Al electroplated onto SiC substrates. Further optimization and improvements will be pursued for both the reflector and substrate, and alternatives such as an Al-alloy substrate will be explored. Some of the key fabrication and integration issues include: bonding and interface between the coating and substrate, environmental overcoats, surface pre- and re-conditioning techniques, and

scale-up issues. In addition, we will develop the techniques necessary to couple the final optic to the target tracking system in order to demonstrate our ability to steer beams and hit targets “on the fly” while maintaining acceptable beam characteristics.

## 1.2. Background

In any laser fusion system, the final optic for each beam is located in the direct line of sight of the exploding fusion targets. Consequently, that optic is exposed to a variety of damage threats. These include prompt neutron and gamma fluxes, x-ray and ionic emissions, and "long" time-scale threats from condensable target and chamber materials, as well as hydrodynamic pressure loads. The potential consequences include increased laser absorption, degradation of the beam quality, and reductions in the laser-induced damage threshold (LIDT).

Three primary goals for damage resistance have been specified previously [1]. We require that the optics operate for 2 years ( $\sim 10^8$  shots) at an incident fluence level of  $5 \text{ J/cm}^2$  (normal to the beam). In-situ reconditioning is allowed if it can be accomplished without significantly degrading the plant availability.

The maximum tolerable level of damage corresponds with 1% increased absorption and uncorrectable degradation of the wavefront by  $\lambda/3$  ( $\lambda=248 \text{ nm}$  for KrF). An increase in absorption equivalent to 1% of the incident beam is likely to result in laser-induced damage to the optic as well as degradation of the spatial profile and increased difficulty balancing the power amongst many beams. The wavefront degradation limit was chosen based on two important target illumination constraints: the spatial nonuniformity of the beam on target must be less than 1% and the spot size and position must be known to within 20 microns. As a rule of thumb, surface aberrations of the order of  $\lambda/3$  will lead to a doubling of the propagation parameter  $M$  [2], which corresponds to a doubling of the diffraction-limited spot size and a doubling of the beam divergence. The allowable wavefront distortion in the final optic depends on the allocation of wavefront distortions throughout the entire optical path as well as the margin for error. Pending further detail on the precise wavefront requirements on target, we are using  $\lambda/3$  as our goal.

Figure 1. shows a design of a GIMM that uses a stiff low-activation substrate (such as C or SiC composite) and a thin aluminum coating on the surface [3]. We have adopted multiplexing of beamlets though each beamline, which leads to an individual optic size of the order of 50 cm. This results in a large number of final optic elements (of the order of 1000), but solves many potential fabrication and operational problems related to cost and quality control, design flexibility, maintainability, spatial variations, compatibility with multiplexed laser amplifiers, robustness due to beam and amplifier overlapping, and opportunities for full scale testing.

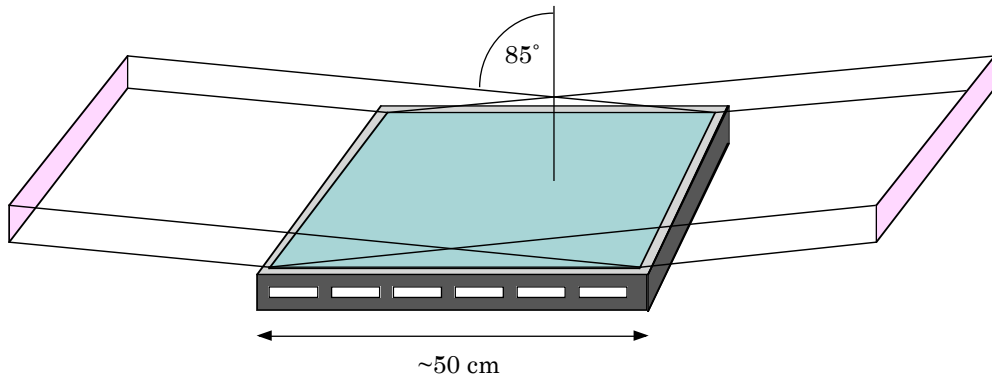


**Figure 1.** Diagram of a grazing-incidence mirror for an IFE power plant

Table 1 summarizes the R&D needs that were identified as important in order to establish the feasibility of this option. In our early research, we concentrated on the basic optical behavior and damage mechanisms. Through the remainder of Phase I, we propose to fill in the database for damage limits, develop and test more prototypical mirrors and also begin to address scaling and system integration issues.

**Table 1.** Key issues for grazing incidence mirrors in IFE [4]

- 
1. Experimental verification of laser damage thresholds
  2. Experiments with irradiated mirrors
  3. Protection against debris and x-rays (shutters, gas jets, *etc.*)
  4. In-situ cleaning techniques
  5. Wavefront issues: beam smoothness, uniformity, shaping
  6. Large-scale manufacturing
  7. Cooling
-

### 1.3. Progress in FY03

During the past year we obtained and characterized both diamond-turned and Al-coated optics (see [Figure 2](#)). Two techniques were used to coat substrates: (1) thin film deposition, and (2) electroplating. Testing was performed using 20-ns pulses from a KrF laser (248 nm). Shot counts up to 100,000 are now routinely obtained in a controlled (vacuum) environment. As a result of testing, the importance of Al coating thickness on polished SiC substrates was clearly demonstrated. When the coating is thinner than the thermal diffusion skin depth, large stresses occur at the interface. This leads to local debonding and eventual destruction of the surface. [5]

For the first time, substrates were prepared using a combination of electroplating and diamond-turning. In order to turn a coated surface, the thickness of the coating needs to be approximately 50  $\mu\text{m}$  or more. Under these conditions, the interface with the substrate is far from the optical surface. In that case, the performance of the reflector is decoupled from the characteristics of the substrate and the requirements on the substrate and interface are greatly reduced. Testing up to 100,000 shots at fluences up to  $10 \text{ J/cm}^2$  was highly successful (see [Figure 3](#)). As compared with solid Al turning, electroplating resulted in much smaller grains, which we believe also contributes to the improved damage resistance. At present, electroplating is our most promising candidate.

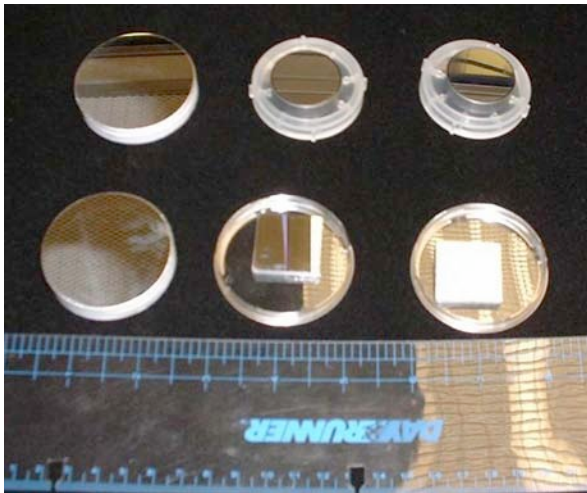


Figure 2. Al mirror specimens tested during FY03



Figure 3. Micrograph of surface electroplated with pure Al, after  $10^5$  shots at  $4 \text{ J/cm}^2$

During testing under rough vacuum, we observed darkening of the surface under the footprint of the beam. This was later shown to be a result of pump oil decomposition stimulated by the UV light. Following this observation, an ultraclean chamber was fabricated and experiments are now performed using a cryopump. As an unexpected side benefit of these experiments, we discovered that carbon was removed from a previously contaminated surface after exposure in a clean chamber. Anecdotal evidence over the past 2 years has consistently shown that contaminants can be removed from a grazing-incidence mirror by the action of the UV laser itself.

Design studies were initiated in order to assess the final optic design requirements and issues related to system integration. For example, mirror segmentation was evaluated in order to set a design-basis size and shape. Beam steering studies resulted in a recommendation to integrate the final target tracking system with the final optic in a confocal geometry. These design concepts are now under evaluation in the target injection and tracking program at General Atomics.

[Table 2](#) lists the tasks that were proposed by UC San Diego for completion in FY03. More details on the outcomes are provided below.

**Table 2.** UCSD Final Optics Tasks Accomplished in FY03

- 
1. Complete the demonstration of grazing angle stability
  2. Expose samples in vacuum and compare with open air irradiations
  3. Obtain coated substrates and demonstrate coating adhesion
  4. Perform experiments to create a database of damage with and without contaminants
  5. Perform experiments to demonstrate acceptable beam quality through exposed optics
  6. Perform ion threat modeling
  7. Perform optical modeling as needed to support experimental activities
- 

1. The basic stability of mirrors at a grazing angle of incidence has been observed through numerous experimental campaigns. Initially we feared that small defects would produce a local perturbation in the angle of incidence, which would absorb light more effectively and grow. On the contrary, we observed a tendency of the laser to smooth out initial defects, especially along the direction of light propagation. Other types of instability have been observed, related to cyclic

inelastic behavior of certain microstructures. We studied large and small grained polycrystalline microstructures, as well as amorphous coatings. Large grains are clearly undesirable; our fabrication studies have focussed on small-grain or amorphous microstructures which appear to be stable.

2. Samples were exposed in vacuum and inert gas, and results were compared with open air irradiations. The absence of oxygen and nitrogen indeed eliminated the dramatic chemical reactions observed previously. However, during vacuum irradiations at high shot count we noticed a darkening of the surface underneath the footprint of the beam. Later studies showed that this was caused by laser decomposition of residual pump oil. Addition of an oil trap did not resolve the problem, so a new cryopumped vacuum system was designed and constructed. Remarkably, specimens which were carbon contaminated were cleaned within about 100 shots after exposure in a clean background gas. Once again, this demonstrated excimer laser cleaning of the surfaces without seeding damage.

3. Coated substrates were obtained and coating adhesion was explored and demonstrated. Previously, our coated substrates contained too many macroscopic defects to allow a well controlled experiment. During the past year we obtained superpolished CVD SiC substrates from Rohm and Haas, and then coated them by sputtering and PVD (e-beam evaporation) at Schafer Corp. We clearly demonstrated the importance of coating thickness. Coatings which are thinner than the thermal penetration depth in all cases were damaged. Ultimately the surface becomes damaged locally at weak points in the substrate. We concluded that no substrate would be sufficiently defect-free to allow for coatings thinner than the thermal penetration depth.

4. Experiments were initiated to create a damage database on electroplated Al on SiC. With our new damage-resistant mirrors, we have been able to increase the shot count up to 100,000. A reference mirror was defined based on electroplated and diamond-turned Al. The damage database now can be filled in for this reference concept. Additional effort will be needed to complete the database.

5. Extensive measurements of surface defects were performed in-situ. We applied imaging, brightfield and darkfield techniques. Emphasis on wavefront quality measurements will continue as we scale up to larger optics.

6. X-ray heating was modeled, indicating the need to implement some mitigation scheme. Ion transport and damage modeling was deferred until FY04. Based on the x-ray modeling results, we are considering the use of gas puffing techniques. We believe that the consequences on chamber clearing, target interactions and impurity mass transport should be assessed before adopting gas puffing as a mitigation scheme.

7. Optical modeling was performed to support experimental activities. Our modeling currently is focussed on the effect of nano-scale precipitates on the optical absorption and scattering, as well as mechanical properties of Al mirrors.

## **2. Task 2: Chamber Dynamics & Clearing**

### **2.1. Statement of Purpose**

Our research aims at developing a fully integrated computer code to simulate and study the dynamic behavior of IFE chamber, including: the hydrodynamics; the effects of various heat sources and transfer mechanisms such as photon and ion heat deposition and chamber gas conduction, convection, and radiation; the chamber wall response and lifetime; and the cavity clearing.

### **2.2. Background**

In a rep-rated laser-fusion facility, the pulse repetition rate is limited by the time it takes for chamber environment to return to a sufficiently quiescent and clean low-pressure state following a target explosion to allow a second shot to be initiated. Laser propagation and beam quality on the target as well target injection and tracking are impacted by the number density, temperature, mix of chamber constituents as well as fluid eddies and turbulence in the chamber.

Many physical phenomena with different time scale occur in the chamber following the target implosion. In the “fast” time scale, x-rays, ions and neutrons from the target implosion travel through the chamber. Depending on the chamber constituents, the x-rays and ions can interact and deposit part of their energy in the chamber. The remaining portion of x-rays and ions arrive at the chamber wall where they deposit their energy. For the case of wetted walls, the wetting agent vaporizes and enters the chamber. In the case of a dry wall protection scheme, photons and ions will interact and affect the surface wall materials in different ways that could result in the emission of atomic (sublimation or vaporization) and macroscopic particles, thereby limiting the lifetime of the wall. Also, mass loss in the form of macroscopic particles can be much larger than mass loss due to the surface vaporization. The “fast” time scale which covers this “first pass” of target x-rays and ions through the chamber can take up to a few microseconds. At the end of this phase, the chamber environment is in a non-equilibrium phase (*e.g.*, non-uniform pressure) and a new source of material is introduced in the chamber.

After this “fast” time scale phase, the chamber environment evolves more slowly, mainly in the hydrodynamics time scale. The aim of the proposed research is to understand the chamber evolution and dynamic over this “longer” time scale and investigate the constraints imposed by chamber dynamics on the laser driver rep-rate.

The focus of our research effort is the development of a fully integrated computer code to model and study the chamber dynamic behavior, including: the hydrodynamics; the effects of various heat sources and transfer mechanisms such as photon and ion heat deposition and chamber gas conduction, convection, and radiation; the chamber wall response and lifetime; and the cavity clearing. Since developing such a simulation capability is a major undertaking, the development of this simulation code is envisioned in several steps of increasing sophistication, *i.e.*, the code will be developed in a modular and staged fashion such that it can be readily and easily upgraded and more detailed physics modules added. In this fashion, the code itself can be used through its development to set priorities – simple models can be added as modules to the code to assess the importance of different processes under different conditions. In addition, utilization of developed expertise in computational fluid dynamics allows us to focus mostly on developing and understanding relevant phenomena. Within these criteria, we initiated development of such a

simulation code under a grant from the Naval Research Laboratory. The code development was implemented in a series of stages with the code being fully functional at the end of each stage. Simulations with each version of the code have been used to plan out the highest leverage directions for implementing physics models and/or numerical algorithms. Our progress to date is described in the next section (Sec. 2.3). The simulation code, SPARTAN, is fully functional and initial simulation results are described below. We have met all milestones to date.

### **2.3. Progress in FY03**

We have developed the SPARTAN chamber dynamics simulation code. The code solves 2-D transient compressible Navier Stokes equations. The code utilizes a state-of-the-art CGF solver package (after Colella, Glaz, and Ferguson) that is based on a second-order shock-capturing Godunov scheme [6,7]. It consists of a robust algorithm for compressible Euler equations and is second-order accurate in regions of smooth flow capturing shocks with a minimum of numerical dissipation and overshoot. CGF algorithm was modified to account for diffusive terms such as viscosity and thermal conductivity.

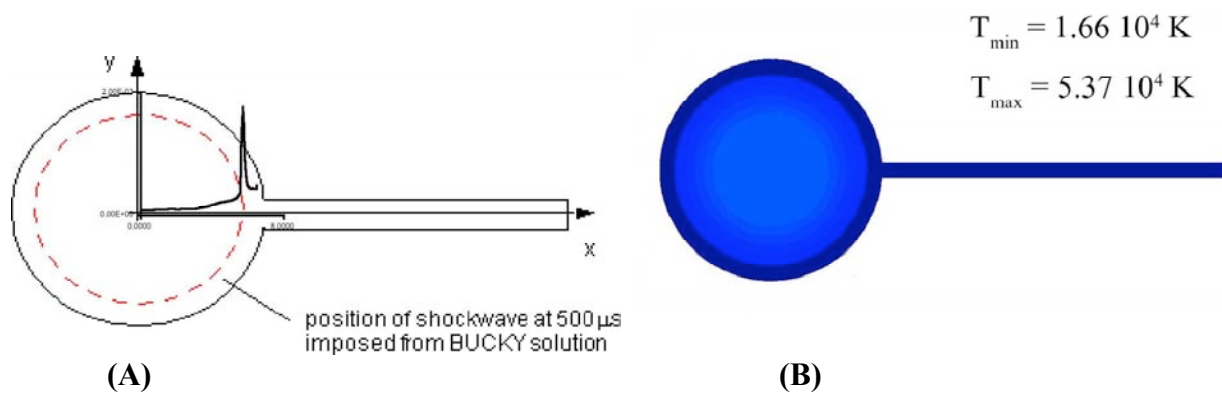
The stage 1 version of SPARTAN was completed last year. Its major features include:

- Code solves 2-D Transient Compressible Navier-Stokes Equations. Extension to 3-D is straight-forward.
- It includes second order Godunov method, for capturing strong shocks.
- It includes Diffusive terms (heat conduction and viscosity)
- Diffusive terms can depend on local state variables (e.g., using Sutherland Law)
- Arbitrary boundary is resolved on a Cartesian grid with Embedded Boundary method.
- Adaptive Mesh Refinement is employed to secure the uniform accuracy throughout the fluid domain.
- Code accounts for heat transfer to the chamber wall (*i.e.*, both zero and non-zero energy-flux boundary conditions)

Some of the simulations performed last year are given below. These simulations were used to highlight and prioritize the physical phenomena and numerical algorithms that should be included in stage 2 of SPARTAN. Programming of SPARTAN v2 code is now completed. Testing of the code and extensive simulations will be performed in the next period as is described below.

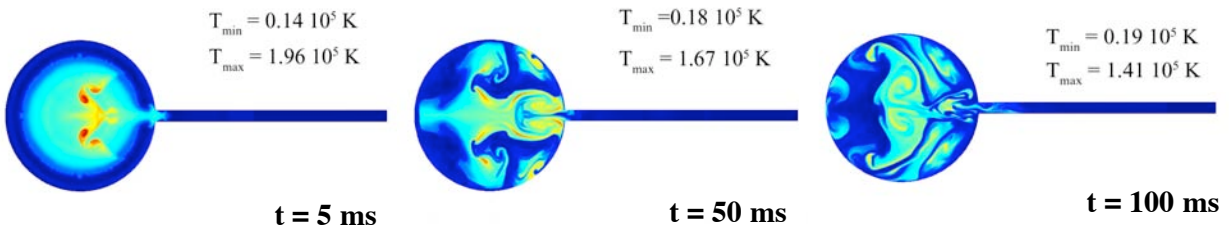
### 2.3.1. Simulation Results

The simulation results below are made for a cylindrical chamber with a radius of 6.5 m. Laser beam channel(s) with a length of 20 m and diameter of 1 m is included to demonstrate the capability of the code to model arbitrary geometry (see Fig. 4). The initial conditions are taken from the BUCKY one-dimensional rad-hydro code 500  $\mu$ s after the target explosion. At this time, the initial shock wave from the target explosion has not arrived at the wall so that chamber geometry does not affect the solution. The one-dimensional BUCKY solution is rotated symmetrically around target explosion point and used as the initial condition. In addition, at this time (500  $\mu$ s after the target explosion), the chamber gas is cooled enough such that chamber gas is transparent to radiation and, therefore, there is no need to include detailed radiation transport models (see Section 2.4 for more discussion).



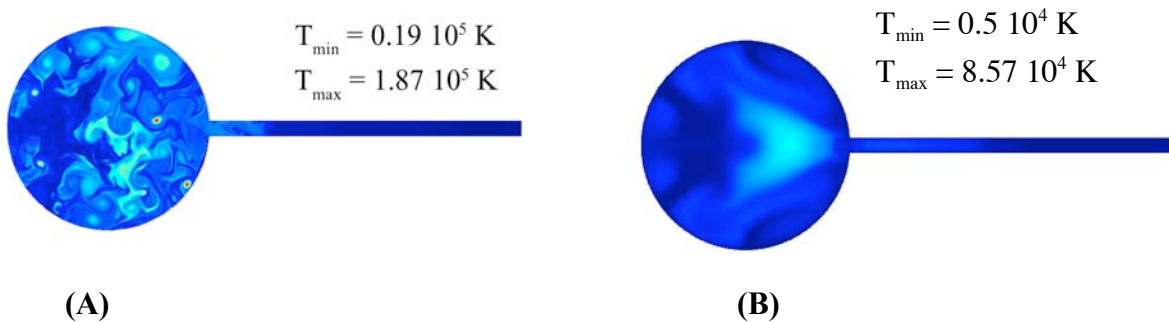
**Fig. 4.** (A) Physical model of simulation domain including the initial condition from BUCKY. (B) Contour of gas temperature in the chamber (both at 500  $\mu$ s after target explosion)

Figure 5 shows a detailed view of color-coded chamber gas temperature contours at different times (full Navier Stocks solution). At  $t = 5$  ms, the shocks generated by target explosion have sufficient time to bounce of the chamber wall and converge back into the chamber center. As can be seen in Fig. 5, this has resulted in two hot spots with temperature reaching 20 eV. By  $t=50$  ms (about 10 shock bouncing time), the shock energy is dissipated and large eddies are set up in the chamber. After this time, the chamber evolves slowly and cools down by conduction into the wall.



**Fig. 5.** Contours of chamber gas temperature at different time after the target explosion.

The importance of diffusive terms (conductivity and viscosity) on the chamber evolution can be seen in Fig. 6. Contours of chamber gas temperature at  $t = 100 \text{ ms}$  after the target explosion are shown. Figure 2.3.A is for the case with NO diffusive terms while Fig. 2.3.B is for the case with full Navier Stocks solution. It is clear that the diffusive terms play a major role in smoothing out chamber environment and reducing chamber temperature and pressure.



**Fig. 6.** Contours of chamber gas temperature at  $t = 100 \text{ ms}$  after the target explosion, A) NO diffusive terms B) full Navier Stocks solution..

The importance of geometrical effects can easily be seen in Fig. 7. Contours of chamber gas temperature at three selected times are shown. In the top row, only one laser beam lines were included. The bottom row includes two sets of laser beam lines. As can be seen, the additional laser beam channel initiates smaller eddies and better mixing in the chamber environment leading to cooler gas temperature at  $t = 100 \text{ ms}$ .

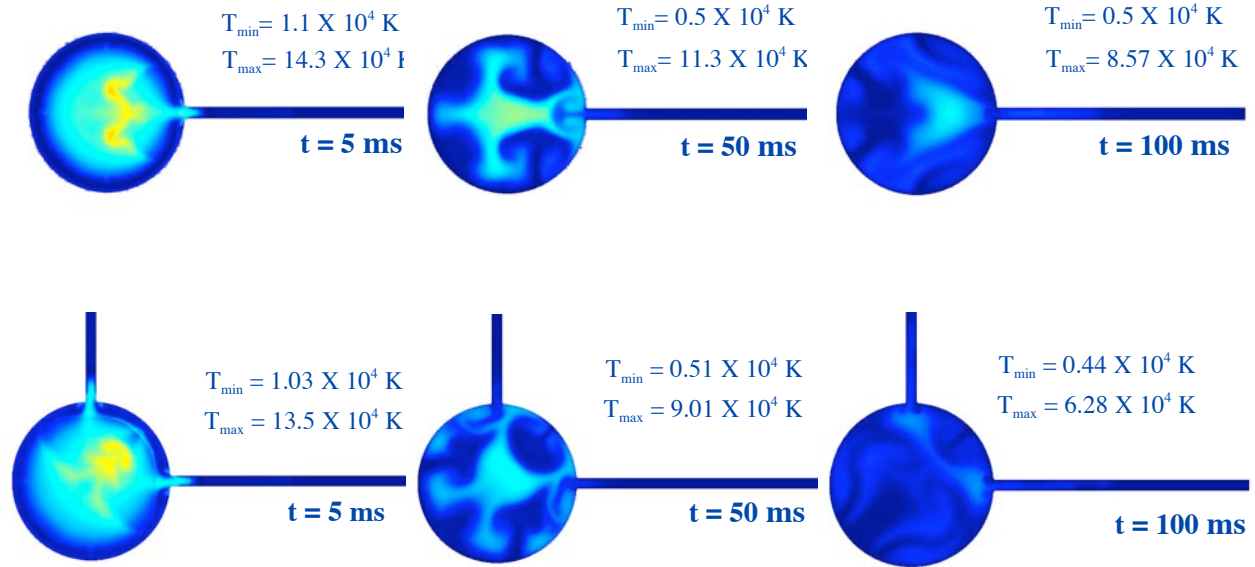


**Fig. 7.** Contours of chamber gas temperature at  $t = 100$  ms after the target explosion (Full Navier Stocks solution). Addition of laser beam channels (bottom row) has led to a better mixing and lower final temperature.

### 2.3.2. SPATRAN upgrades

Based on the results from SPARTAN simulation, the following upgrades were implemented:

1) We have introduced a new splitting scheme for the diffusive terms, *i.e.*, diffusive terms are included now as source/sink terms in both predictor and corrector steps of numerical algorithm. As a result, SPARTAN is now formally second-order accurate in the whole domain for any Reynolds number. This improved convergence has resulted in a factor of two reduction in the simulation time. In addition, this new algorithm allows extension of to multi-species capability because source and sink terms are now formally included in the algorithm.

2) We have improved our embedded boundary algorithm such that it is also formally second order accurate.

3) At present, SPARTAN assumes uniformity in  $z$  direction (perpendicular to the plane of solution), *i.e.*, the model problem of Fig 4 represents a long cylinder. In this way, the laser beam

channels in Figs. 4 to 7 are actually “slots” as opposed to tubes. Because of the observed importance of geometrical effects in SPARTAN simulation, we have implemented numerical algorithms so that SPARTAN can now solve problems with cylindrical symmetry. This, for example, allow for simulation of spherical chambers and/or cylindrical chambers with cylindrical beam channels (only at the two ends).

4) SPARTAN simulations showed that (see, for example, Fig. 5) shocks generated by target explosion bounce of the chamber wall and converge back into the chamber center forming hot spots. The temperature at these hot spots is sufficiently large that a substantial ionized material will exist in the chamber. Electron thermal conduction and radiation from this background plasma can help cool the chamber gas substantially. Estimates indicate that at densities and temperatures of interest, the chamber gas is transparent to radiation. As such, a reasonably accurate and simple method to account for the background plasma is to assume that the chamber constituents are in coronal equilibrium and computer electron density, temperature (and thermal conduction and radiation heat fluxes). Such a model is incorporated in SPARTAN and is undergoing testing at present.

### **3. Task 3: Experimental studies of laser-IFE chamber wall**

#### **3.1. Statement of Purpose**

Our research aims at developing and testing candidate material for the wall of laser-IFE chambers that can accommodate the laser IFE threat spectra and provide the required lifetime.

#### **3.2. Background**

Predictive capability of the IFE chamber response requires a detailed understanding of the response of the chamber wall as the wall response dictates the constituents of the laser IFE chamber:

1. Properties of the chamber buffer gas (*e.g.*, type and density) are dictated by the survivability of the chamber wall,
2. Material ejected from the wall represent a major portion of material in the chamber

Most of the research previously has focused on wall mass loss due to sublimation. For a given x-ray and ion flux on the wall, temperature evolution of the wall is computed for perfectly flat wall using steady state and bulk properties for pure material. Mass loss is then estimated based on sublimation and/or melting correlations. These analyses indicate that the temperature variation mainly occurs in a thin region ( $<100 \mu\text{m}$ ) and large temperature gradients are limited to first few (or ten) microns. Beyond this region, the first wall experiences a much more uniform heat flux. As such, we proposed two years ago to use a thin armor instead of a monolithic chamber wall. Armor can then be optimized to handle rapid particle and heat flux while the first wall is optimized for structural function and efficient heat removal at quasi-steady-state. In addition, in an IFE power plant, most of the neutrons are deposited in the back where blanket and coolant temperature will be at quasi steady state due to thermal capacity effect. As such, most first-wall and blanket concepts developed for MFE will be directly applicable to IFE applications. There are several possibilities for armor material: 1) W and other refractory metals, 2) Carbon (and CFC composites), and 3) more exotic engineered material. Each has its own set of potential advantages and critical issues that should be addressed with rigorous R&D. In particular, means for in-situ repair of the armor should receive special attention.

There are a large number of uncertainties associated with the armor:

#### **A. Material loss due to increased wall temperature (e.g., evaporation, sublimation)**

1. Surface features in a practical system are typically larger than tens of microns and impurities and contaminants can cause hot spots. As such, wall temperature estimates are highly uncertain.
2. Sublimation is extremely sensitive to material temperature and partial pressure. Accurate knowledge of wall temperature is essential in sublimation estimates. Steady-state data for sublimation rates may not be applicable to fast transients in the chamber wall. Sublimation at local hot spots (contaminants, surface morphology) material loss due to contaminants on the surface may be important. Examples include formation of WC on the wall which has a melting point much lower than W or formation of CH on the wall that can vaporizes at very low temperature.

#### **B. Failure due to Thermomechanical loads**

1. Rapid differential thermal expansion caused by thermal shock can cause catastrophic failures of armor and back wall.
2. Rep-rated thermal expansion and resulting stresses can lead to armor failure due to thermal fatigue.

3. The joint between armor and back wall can fail due to rep-rated thermal expansion and fatigue.
4. It is possible that significant material loss does not occur for metallic armors even if a small layer of armor melts during each shot. Melting and solidification of this melt year may have adverse (loss of strength) or positive (removal of defects) in thermomechanical response of the armor.
5. Contaminants and impurities can impact the armor response to any of the above mechanisms.

### **C. Material loss due to ion and neutron bombardment**

1. Neutron irradiation affects the thermophysical properties of the armor material. While full resolution of this issue awaits construction of intense 14-MeV neutron source (corresponding to expected fusion neutron spectrum from the exploding target), some insight is gained through test in fission reactors.
2. Severe ion bombardment of the armor material could lead to massive material loss. For example, implantation of He ions in particular in W (in which He diffusion is very poor) can result in a 1 to 1 ratio of W to He within about 100 days of operation assuming a 1  $\mu\text{m}$  implantation depth. This would lead to severe blistering of armor and must be remedied by solutions such as operation at high enough temperature for He to be mobile in W or by using very fine porous structure providing a very short diffusion path for He to be transported to open porosity and back to the chamber. The above experimental observations are for mono-energetic ions in which all ions come to rest at the same location in the material. The ions arriving at the IFF chamber wall have a range of energies and, therefore, calculations show that this issue may not be a large concern. Experiments are needed to confirm this theoretical prediction.

As a source with integrated and prototypical spectrum of x-rays and ions is not available, experiments should be performed in simulation facilities. Our analysis indicates that most of phenomena leading to the failure of the wall depend on wall temperature evolution (temporal and spatial) and chamber environment; only sputtering and radiation (ion & neutron) damage effects depend on “how” the energy is delivered. Several means for delivering energy in ns time-scale are available: lasers, x-ray sources, electron beams, and ion beams. Lasers provide a “clean” source of energy for wall simulation experiments. Irradiation of wall samples with lasers does not impose any constraint on the experimental chamber and, thus, make is relatively easy to field diagnostics. We have shown that a 10-ns laser pulse can simulate temperature evolution in the wall sample that is prototypical of laser IFE chambers response to x-rays (see [Figure 7](#)). Peak wall temperature and temperature gradients in the wall can be easily adjusted by controlling the laser energy and/or modification of laser pulse shape. In addition, relatively low-cost laser

system can produce sufficient rep-rate to easily investigate wall response to  $10^6$  shots. This is especially an attractive option as existing YAG laser at UCSD can be used for this purpose.

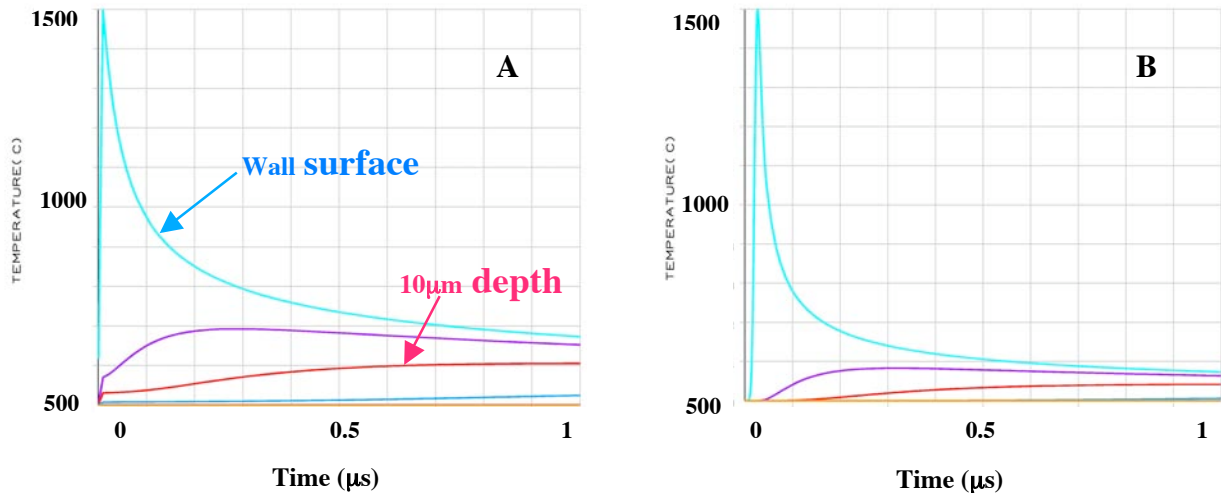


**Figure 7.** Temperature history in a tungsten flat wall subjected to a) NRL direct-drive target x-ray channel and b) a 10 ns Gaussian laser pulse. Temperature evaluation on the surface and at depths of 5, 10, and 20 microns are shown. Only the laser energy is adjusted such that similar peak wall temperature ( $\sim 1500$  C) is achieved in the simulation experiments.

Ion sources are considerably more expensive but they would provide additional data, as the primary energy release channel in direct-drive capsules is the ion channel. The existing RHEPP facility at Sandia has been used to study wall response. The drawback of this facility is its low rep-rate and the fact that ion spectrum is not similar to that expected from an IFE target explosion. In addition, special diagnostics has to be fielded on RHEPP to measure temperature evolution of sample in real time. Overall, our conclusion is that laser provides the most flexible and low-cost option to investigate laser-IFE chamber wall response. Similar simulation experiments (but at low rep-rate, with small number of shots, and smaller suite of diagnostics) can be fielded in RHEPP facility. The combination of two efforts provides a large body of experimental database for laser-IFE wall research. In particular, comparison of experimental results from a laser facility with similar experiments performed in RHEPP will underline if the wall failure mechanism is mainly due to temperature evolution and/or other effects can be important.

### 3.3. Progress in FY03

Under Grant from Naval Research Laboratory, we have designed and built a simulation experimental facility to determine thermo-mechanical response of the chamber wall. An illustration of the experimental set-up is shown in [Figure 8](#). The energy source is our existing 2 J (at 1 micron) Nd-YAG laser. It can operate at 10-HZ allowing rep-rated experiments ( $10^6$  shots per day), if necessary. Our laser includes injection seeding for reproducible and smooth temporal profiles. We have utilized an existing vacuum chamber with inside dimensions of 10"x12". Our vacuum system is capable of pressures below  $10^{-8}$  torr and includes a gas feed system to inject a mixture of four types of gases in the chamber to simulate chamber environment and contaminants. Experimental set up is mounted on an optical breadboard and placed in the chamber.

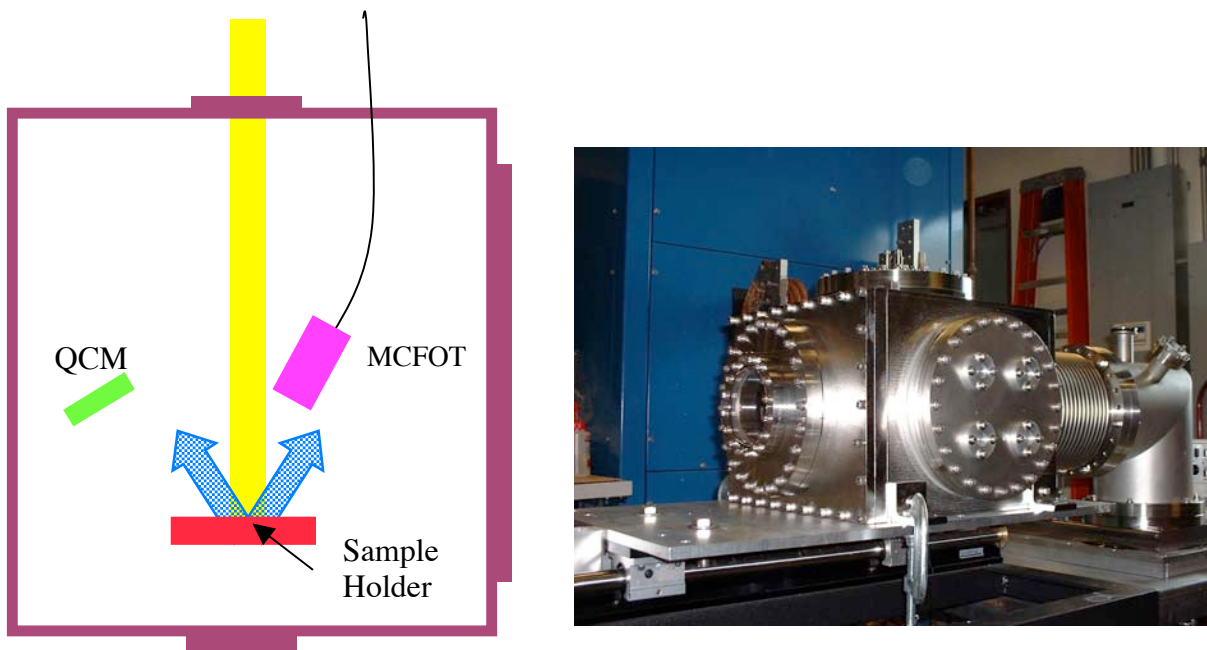


**Figure 8.** Schematic of simulation experiments of the chamber wall. The existing vacuum vessel is also shown.

The thermomechanical response of the armor depends strongly on the equilibrium temperature of the armor between shots. For IFE chambers, equilibrium wall temperature ranges from 600 to over 1000 °C. During last year we designed, built and fielded a high-temperature sample holder which can maintain the equilibrium sample temperature from room temperature to 1,200 °C.

This sample holder operating at 1,000 °C is shown in Fig. 9. Endurance runs of several runs at 1,200 °C have been performed to demonstrate the reliability of the sample holder.

In calendar year 2003, we have purchased and installed a residual gas analyzer (RGA) and a Quartz-Crystal Micro-balancing (QCM) systems. These systems will allow detailed measurement of mass loss from the sample armor material

In order to correlate experimental results with computations and develop a predictive capability, accurate measurement of sample temperature evolution during the shot is necessary (nano-second resolution). Most of activity in 2003 was devoted to development of a fast optical thermometer with nano-second temporal resolution.

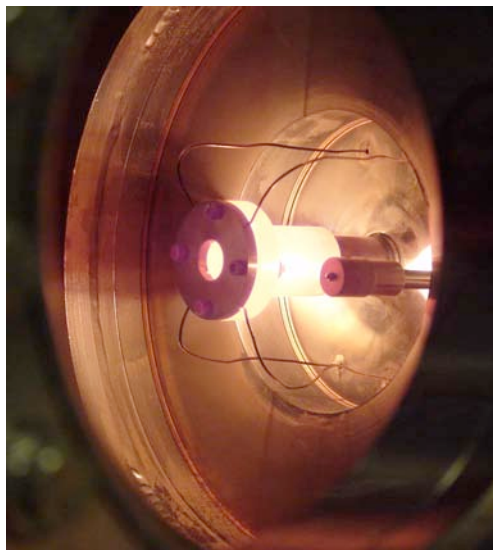


**Figure 9.** Photograph of sample holder operating at 1,000 °C inside the experiment chamber.

Optical thermometry is probably the only way to measure temperature of hot surfaces with nano-second resolution. All optical thermometry schemes are based on the fact that any body will radiate energy according to Planck's Law. The radiance (radiant intensity emitted by a source per unit projected area of the source in the wavelength range of  $\lambda$  and  $\lambda + d\lambda$ ) is given by:

$$L_{\lambda} (T) = \frac{2}{\lambda^5} \frac{c_1}{\exp(c_2/\lambda T) - 1}$$

Where  $\epsilon$  is the emissivity of the material,  $T$  is temperature in K and  $c_1$  and  $c_2$  are constants. The total emitted radiation from the source can be found by integrating the radiance over all wavelengths. For low-temperatures, below 500-700K, thermal radiometers are used which measure the total radiation from a surface (cheaper devices) and/or radiance in a certain infra-red frequency. Because the emissivities of most material at low temperature are between 0.9 to 0.95, the emissivity,  $\epsilon$  in the above formula is usually ignored. In addition, most thermometers have, at best, millisecond temporal resolution.

At higher temperatures, (*e.g.*, 2,000-4,000 K), emissivity is a strong function of temperature and, to some extent, the wavelength (or color). Deduction of surface temperature from the measured radiance requires a priori knowledge of the emissivities. Two-color method is usually used when the emissivities are unknown. In the two color method, the radiances at two wavelength,  $\lambda_1$  and  $\lambda_2$  are measured. Assuming that  $\epsilon(\lambda_1, T) = \epsilon(\lambda_2, T)$ , the temperature can be deduced from the two radiant intensities. This is a very good assumption especially if  $\lambda_1$  and  $\lambda_2$  are close to each other. Two-color method has been used successfully, for example, to measure the temperature of flame-fronts in combustion research. We have developed such a two-color optical thermometer which operates with a nano-second resolution.

Schematic of the two-color optical thermometer is given in [Fig. 10](#). Published work on multi-color optical thermometry were limited to response time of millisecond to micro-second. In addition, they include complicated optical trains that would be difficult to implement in the experimental chamber. Our system can be mounted into a vacuum chamber and has a temporal resolution of better than 1 ns (limited at present by the response time of the fast oscilloscopes used). The system consists of two parts: the thermometer head and detector assemblies. These two parts are connected by fiber optic. As such, they can be placed at a convenient distance from each other, for example the head can be mounted in a vacuum chamber while the detector is located outside. The thermometer head includes a collimator/focuser optical train which images the hot surface into a fiber optic. In principle, we can image areas smaller than 100  $\mu\text{m}$  (*i.e.*, thermometer has a spatial resolution of  $< 100 \mu\text{m}$ ). Light from the head is carried by the fiber optic to the detector assembly. In the detector, the light is split into two beams. Notch filters are

used to choose the desired wavelengths for each beam. The radiances at those wavelengths are, then, measured by photo-multiplier tubes (PMT). A fast oscilloscope measures the voltages from the PMTs. A PC downloads the data from the scope and makes the necessary computations and displays the temperature profile. We have calibrated our thermometer using an absolutely calibrated Optronic UL-45U lamp with a total error of  $< 1.5\%$ .

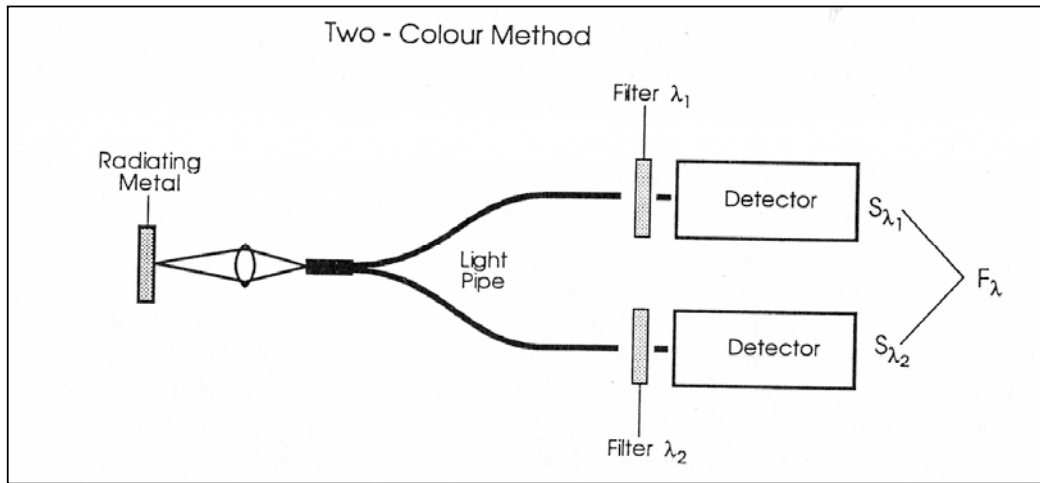


**Figure 10.** Schematic of Two-color Optical Thermometry

Figures 11 and 12 show experimental results from our optical thermometer. In these experiments, a tungsten sample was irradiated by a Nd:YAG laser with a pulse length of  $\sim 8$  ns. The laser energy was varied and was increased until the sample surface was melted. Figure 11 shows the temperature profile for a case when laser energy was sufficiently high to melt the sample surface. As can be seen, the sample temperature reaches 3,700K (melting point of tungsten) and remains there for 2 ns before decaying. In this figure, the thermometer was “tuned” to measure temperatures between  $\sim 2500$  K and 4000 K. Depending on the sensitivity of PMTs used, we have been able to measure surface temperatures down to about 1700 K.

Figure 12 shows a scan of maximum temperature of the W surface as a function of laser energy. It shows a linear rise initially as expected (adiabatic heating of sample surface). The surface temperature, then, remains at the melting point when laser energy is increased further.

Extensive reliability tests have been performed. These tests demonstrated that the thermometer holds its calibration over a two-week period (duration of the reliability tests). These tests

included simulated test of steps needed for moving the head assembly from calibration stand into the vacuum chamber (and pump down) as well as partial disassembly of the both thermometer head and detector assemblies.

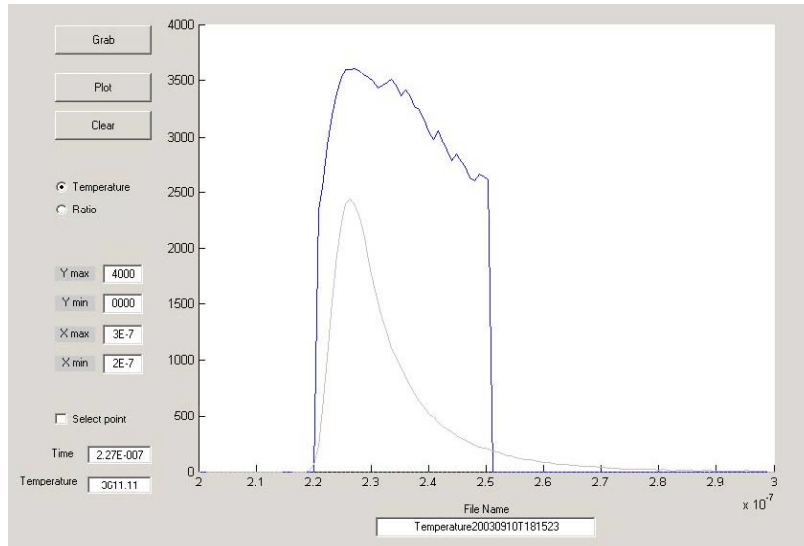


**Figure 11.** Temperature profile of a tungsten sample irradiated with 600 mJ of laser energy sufficient to melt the sample surface.

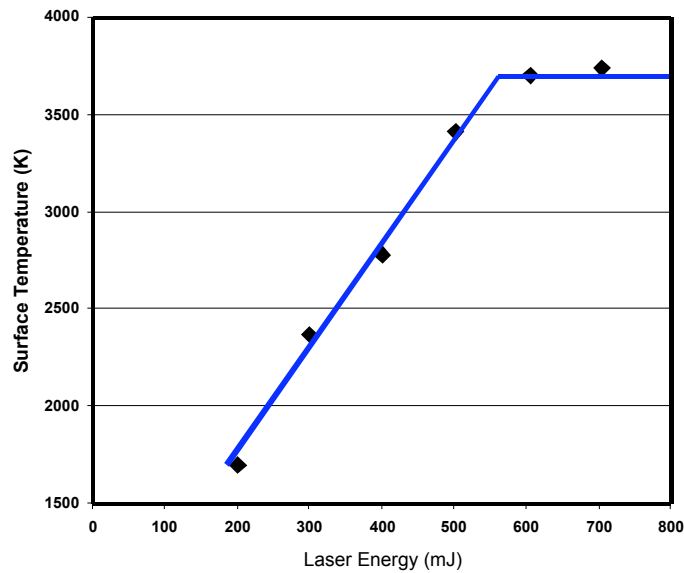


**Figure 12.** Scan of maximum surface temperature as a function of laser energy.

## References:

1. M. S. Tillack, S. A. Payne, N. M. Ghoniem, M. R. Zaghoul and J. F. Latkowski, "Damage threats and response of final optics for laser-fusion power plants," Inertial Fusion Science and Applications 2001, Kyoto Japan, Sept. 2001.
2. C. D. Orth, S. A. Payne, and W. F. Krupke, "A Diode Pumped Solid State Laser Driver for Inertial Fusion Energy," *Nuclear Fusion* **36** (1996) 75-116.
3. L. M. Waganer, "Innovation Leads the Way to Attractive IFE Reactors – Prometheus-L & Prometheus-H," IAEA Technical Committee Meeting and Workshop on Fusion Reactor Design and Technology, 13-17 Sept. 1993.
4. R. L. Bieri and M. W. Guinan, "Grazing Incidence Metal Mirrors as the Final Elements in a Laser Driver for Inertial Confinement Fusion," *Fusion Technology* **19** (May 1991) 673-678.
5. M. S. Tillack, J. Pulsifer and K. Sequoia, "UV Laser-Induced Damage to Grazing Incidence Metal Mirrors," Inertial Fusion Science and Applications 2003, Monterey CA, Sept. 2003 (to be published).
6. G. H. Miller and E. G. Puckett "A high-order Godunov method for multiple condensed phases," *J. Comput. Phys.* **128** (1996) 134.
7. Marcus Day, Center for Computational Sciences and Engineering at Lawrence Berkeley National Laboratory, private communications.